International Journal of Fatigue 126 (2019) 346–356

Contents lists available at ScienceDirect

International Journal of Fatigue

journal homepage: www.elsevier.com/locate/ijfatigue

Fatigue crack initiation and propagation behavior in Al – 7075 alloy under in-phase bending-torsion loading

Abhay K. Singh[a], Siddhant Datta[a], Aditi Chattopadhyay[a,*], Jaret C. Riddick[b], Asha J. Hall[b]

[a] School of Engineering for Matter, Transport and Energy, Arizona State University, Tempe, AZ 85287, USA
[b] Vehicle Technology Directorate U.S. Army Research Laboratory, Aberdeen Proving Ground, MD 21005, USA

ARTICLE INFO

Keywords:
Multiaxial fatigue
Bending-torsion
Crack initiation
Crack propagation
Fractography

ABSTRACT

Fatigue crack initiation and propagation behavior were investigated on a tubular specimen of Al 7075 alloy subjected to multiaxial mixed mode bending-torsional loadings. Tests under pure bending and pure torsional loadings were also conducted to segregate the effect of multiaxiality. A single crack nucleated on the plane of maximum shear stress in all the tests, except for pure torsion. For pure bending, crack propagated on the plane of maximum shear stress in a mixed mode condition tracing an inverted S-shaped trajectory; whereas, crack trajectory under combined bending-torsional load consisted of mode I dominant region, transition region, and pure mode II region. Furthermore, analyses of fracture surfaces were conducted to determine the micro-mechanisms governing crack initiation and propagation behavior.

1. Introduction

The use of damage tolerance design concepts and increased demand for accurate residual fatigue life predictions of airframe structures have led to the growing need for the study of fatigue damage initiation and propagation under realistic multiaxial fatigue loading scenarios. Multiaxiality can arise from several factors, such as multiaxial external loading, complex geometry, residual stresses, crack orientation, etc. Many research studies in literature focus on crack growth under pure mode I and/or mode II loading conditions [1–4]. However, many service failures occur from components being subjected to mixed-mode multiaxial fatigue loadings. A typical example of external loading in engineering application is a crack initiated in a transverse plane from a tubing shaft surface under combined bending and torsional load [5]. Components of rotorcraft and fixed-wing aircraft also undergo bending-torsion coupled fatigue with varying values of stress amplitude ratio. Similarly, pressure vessels, tubes, and pipes are subjected to biaxial stresses due to internal pressure. Transmission shafts in automobiles experience combined shear stresses arising from torque and axial stresses generated by bending [6]. In practical applications, structures and components are often subjected to complex multiaxial loadings where ideal conditions don't exist, and the naturally initiated fatigue cracks grow in a mixed-mode manner [7]. Since a fatigue crack under mixed-mode condition propagates in a non-self similar manner, predicting the crack path or quantifying crack growth throughout various stages in its propagation involves several complications. Under such conditions, estimation of fatigue life and/or monitoring crack growth is not only a challenging task but also cumbersome. Therefore, it is important to investigate the characteristics of fatigue damage under such complex loading conditions in order to accurately estimate their service life, damage initiation, and crack growth behavior.

The majority of investigations on nucleation and propagation of fatigue damage have been conducted under uniaxial load conditions [8]. In the limited studies conducted on multiaxial loading, primary attention has been given to investigate axial-torsion coupling, in which either both the loadings were cyclic or one of them was cyclic while other was static [9,10]. Very few investigations have been reported on the fatigue behavior of metallic materials subjected to combined bending and torsional loadings [11–19]. Perhaps, Gough et al. [11] were the first to study the combined effect of bending and torsional load using a solid cylindrical bar of steel. Loads were applied with the help of intricate fixture design, in which a single loading arm was used to transmit the combined load to the specimen by adjusting the angle of orientation between the arm and the specimen. Thus, the mismatch in orientation was utilized to split the applied load into two components, i.e. bending moment and twisting moment. Similar test set-up was used in the subsequent experiments by different authors in their research work [17–19]. Findley et al. [17] studied the behavior of 76S-T61 aluminum alloy for four different combinations; Marciniak et al. [18] used two different grades of steels (18G2A and 10HNAP); Niesłony

* Corresponding author.
E-mail address: aditi@asu.edu (A. Chattopadhyay).

https://doi.org/10.1016/j.ijfatigue.2019.05.024
Received 9 April 2019; Received in revised form 15 May 2019; Accepted 20 May 2019
Available online 22 May 2019
0142-1123/

Nomenclature

P_{max}	maximum bending load
P_{min}	minimum bending load
T_{max}	maximum torsional load
T_{min}	minimum torsional load
R	load ratio ($\frac{P_{min}}{P_{max}}$ or $\frac{T_{min}}{T_{max}}$)
N_f	fatigue life
τ_T	shear stress due to torsional load only
τ_{max}	maximum shear stress due to torsional and bending loads
σ_b	maximum tensile stress due to bending load only
SIF	stress intensity factor
K_I	SIF for pure mode I
K_{II}	SIF for pure mode II
λ	stress amplitude ratio ($\frac{\tau_T}{\sigma_b}$)
ϕ_M	mode mixity ($\tan^{-1}\frac{K_{II}}{K_I}$)
L	length of mode I dominant crack
L_{avg}	average length of mode I dominant crack
θ	orientation of mode I dominant crack
θ_{avg}	average orientation of mode I dominant crack
r	radius of curvature for crack deflection

et al. [19] investigated the behavior of AA 6068 and AA 2017A. All these studies [16–19] were conducted on solid cylindrical specimens using stress-life approach in order to determine fatigue life or endurance limit but none of the reported results provide any information either on the damage initiation mechanisms or on the crack propagation behavior of the materials under investigation, which are the two crucial aspects in the analysis of fatigue crack under mixed mode loading.

There is very limited experimental data available on combined bending-torsion fatigue that describes damage initiation or crack propagation behavior in the material [12–15]. Susmel et al. [12] studied the fatigue behavior of solid cylindrical Al 6082-T6 under fully reversed bending-torsion condition and found that when bending dominates in the loading ($\lambda < 1$), the crack initiation occurs in mode II at a point of maximum bending load, but the crack primarily propagates under mode I stresses On the other hand, when the applied torque is dominant ($\lambda > 1$), multiple cracks nucleate on the gauge surface and are oriented along the extrusion direction. These observations remained consistent irrespective of the phase difference in the loading. Park et al. [13] investigated the behavior of small crack in A533B steel for in-phase and 90° out-of-phase loading and found that the crack growth rate varied linearly with the crack size. For all the cases, cracks initiated on the plane of maximum shear strain, but propagated differently for in-phase and 90° out-of-phase loading. While the crack continued to grow on the plane of initiation for 90° out-of-phase loading, it transitioned from the plane of maximum shear strain to the plane of maximum normal strain for in-phase loading as the strain level or the ratio of shear-to-bending strain was reduced. Some researchers have also used notched specimen in their study [14,15]. Park et al. [14] used solid round bars of steel with a circumferential semicircular groove and found that the cracks nucleated on the planes of maximum amplitude of shear stress, but propagated on the planes of maximum principal stress amplitude. An exception to this trend was observed for 90° out-of-phase tests when $\lambda < 0.5$, for which crack propagated on the planes oriented between the planes of maximum shear stress amplitude and the planes of maximum principal stress amplitude. Branco et al. [15] studied fatigue behavior of lateral notched round bars made of high strength steel and found that multiple cracks were nucleated on the fracture surfaces. With an increase in either normal stress amplitude or λ, early initiation of the crack was observed along with an increased rate of crack propagation. In the aforementioned studies, little attention was given to study the nature of crack initiation and propagation behavior under combined bending-torsional loading, and there is a significant lack of understanding into the underlying fatigue-fracture micromechanisms. In addition, all the investigations on bending-torsion loading till this date have been performed on specially designed complex test setup, which precluded the attainment of consistency in the test procedure, and complicated the load applying mechanism, making it less reliable. Since it is evident that the fatigue damage nucleation and crack propagation behavior depend on a multitude of factors, such as material properties, stress amplitude ratio, applied load, phase difference, presence of notch, etc., it becomes imperative to investigate crack behavior under combined bending-torsional loading. To the authors' knowledge, there is no reported literature on the behavior of Al-7075, a high-strength aluminum alloy often employed in aerospace components, under complex multiaxial bending-torsional loading.

This paper presents a macroscale and a microscale experimental investigation of fatigue damage behavior in tubular specimens of Al-7075 subjected to multiaxial in-phase bending-torsional loading with the help of a simple test setup. The primary goal is to obtain a comprehensive insight into fatigue damage initiation, crack orientation & trajectory, crack deflection, and crack propagation modes at various magnitudes of applied load, and stress amplitude ratio. A detailed microscopic analysis of the fracture surfaces is conducted that reveals distinct fracture features and active micromechanisms operating along the direction of crack propagation at various stages in its propagation. The effect of load magnitude and/or stress amplitude ratio on micromechanism governing crack nucleation and propagation are also identified and characterized.

2. Material and methods

2.1. Material

The material used in this bending-torsional fatigue study was procured in the form of cylindrical bars of aluminum alloy 7075-T6, which is often used in aircraft structural components, automotive industry, and other high-strength applications [20]. Material properties provided by the manufacturer include a yield strength of 503 MPa, the ultimate tensile strength of 572 MPa, and modulus of elasticity of 71.7 GPa. It has Brinell hardness value of 150 and the chemical compositions are in accordance with ASTM standard B211.

2.2. Specimen and fixture design

Specimen design plays an important role in investigating the fatigue crack initiation and propagation behavior, and there is no standardization of specimen geometries for testing mixed-mode loading conditions. Richard [21] has presented nine different specimens, which are often used in mixed mode fracture and fatigue studies. These include: plate specimen with inclined central crack under tension, plate specimen with inclined edge crack under tension, disc specimen with inclined central crack, cruciform specimen with inclined central crack, shear specimen with inclined central crack, tubular specimen with inclined crack under torsion, tubular specimen with transverse crack under combined tensile and torsional stresses, three or four point bending and shear specimen with an offset edge crack, and compact tension and shear specimen. In case of experiments involving torsion, either a solid cylindrical specimen or a tubular specimen is used. It is an established fact that a thin-walled tubular specimen is an efficient way to produce mode II crack growth under completely reversed torsional load. On the other hand, circumferentially notched cylindrical specimens are found to be more useful in studying fatigue crack growth behavior during mode III loading [5]. For a mixed mode load condition,

involving bending and torsion, it is advantageous to use a tubular specimen since a crack initiated in a transverse plane from a tubing shaft surface under bending and torsion is under a state of combined mode I, II and III loadings [5]. An added advantage of a tubular specimen over a solid cylindrical specimen is that the solid cylindrical specimen is subjected to a stress gradient along the specimen thickness and an ideal biaxial stress state is not obtained; therefore, a tubular specimen is adopted for investigating mixed mode bending-torsion fatigue behavior and analysis is conducted to validate the state of stress.

In this experiment, a tubular specimen is used, which was machined from solid bars of aluminum alloy (Al 7075-T6). The specimen, as shown in Fig. 1, was designed in compliance with ASTM standard E2207-15 while the length of the gripping area was increased to 250 mm to accommodate the specimen into the test frame. The selected standard provides design recommendations for a thin-walled tubular specimen under axial-torsional load coupling and it also fulfills the design requirements for the specimen under combined bending-torsion loading. As shown in Fig. 1, the specimen has a gauge length of 30 mm in the central part, where outer and inner diameters are 20 mm and 17 mm respectively, making it possible to have a relatively thin wall (1.5 mm thickness).

A suitably designed fixture was required by the vertical actuators to apply bending load on the designed specimen. As shown in Fig. 2, the fixture was designed to accommodate the curved shape of the specimen, while distributing the bending load over a length of 7 mm along the longitudinal axis of the specimen. A CAD package (SOLIDWORKS) was utilized during the entire process to complete the fixture design.

2.3. Experimental procedure

Experiments were conducted using the MTS planar biaxial/torsion load frame with a dynamic load capacity of 100 kN in both horizontal and vertical directions and torsional capacity of 1100 Nm. The load frame is equipped with six independent controllers that allow the users to conduct tests under a wide range of load conditions, including in-phase, out-of-phase, proportional and non-proportional loading. As shown in Fig. 3, the two horizontal actuators were used to apply torsional load while the bending load was applied with the help of a specially designed fixture mounted on one of the vertical actuators. Fatigue tests were conducted for both uniaxial (pure bending / pure torsion) and multiaxial (combined bending and torsional) load conditions, which are summarized in Table 1. All the multiaxial in-phase bending-torsional fatigue tests were carried out at a constant value of stress amplitude ratio ($\lambda = 0.6$) at room temperature. The value of λ was selected such that the fracture phenomenon comprised the effects of both torsion and bending loads at different sets of load conditions (Load 1–Load 3) used in the experiments. For each set of loads, 3–5 specimens were tested using constant amplitude sinusoidal loads at a frequency of 1 Hz and a load ratio (R) of 0.1, the details of which are presented in Table 1. Table 1 also contains the details of the tests conducted under pure bending (Load 4) and pure torsion (Load 5) load conditions. These tests were conducted to evaluate their individual contributions on crack propagation behavior and on fatigue life to better understand the effect of multiaxiality under combined bending and torsional loading. A high-resolution camera was positioned on the rear side of the specimen to capture the crack initiation and growth. The camera was programmed using LabVIEW to capture images at user-defined time intervals. The fatigue tests were interrupted once the surface crack length reached approximately 10–15 mm or if the crack has traveled completely through the thickness of the specimen for a length of 3–6 mm. For the microscale analysis of crack initiation and propagation behavior in Al 7075-T6, fracture surfaces were studied using a scanning electron microscope (SEM).

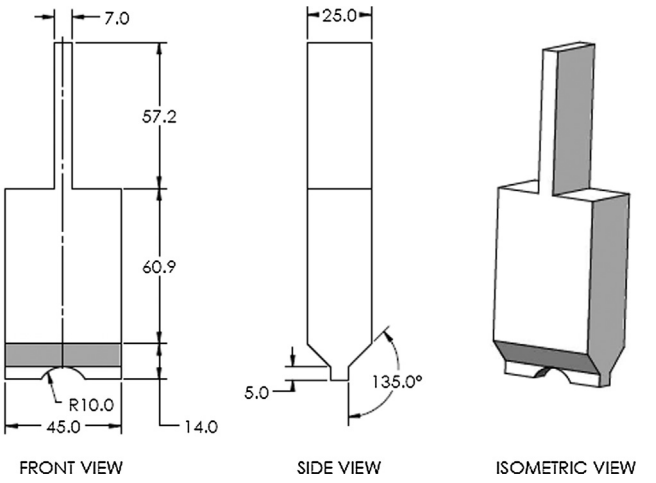

Fig. 2. A specially designed fixture to apply bending load during pure bending and combined bending-torsional loading. All dimensions are in mm.

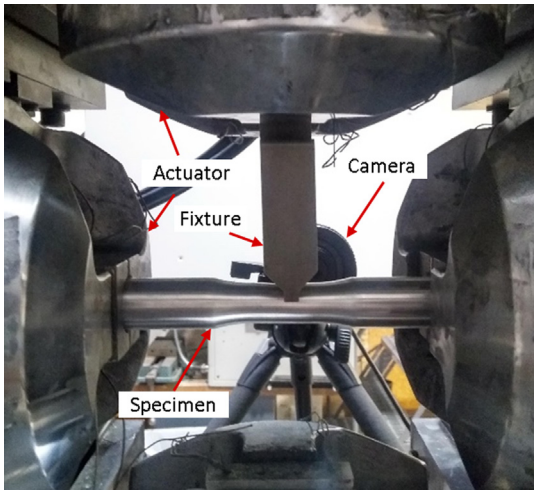

Fig. 3. Experimental set-up used in conducting fatigue tests under various load conditions.

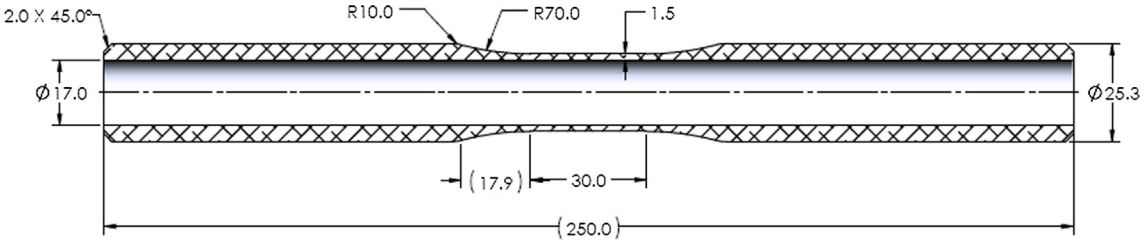

Fig. 1. Design of tubular specimen used in fatigue testing under pure torsion, pure bending, and combined bending-torsional load conditions. All dimensions are in mm.

Table 1
Details of fatigue test conducted under different loading conditions.

Load Case	Test ID	R-Ratio	P_{max} (N)	T_{max} (N.m)	Frequency (Hz)	τ_T (MPa)	σ_b (MPa)	λ (τ_T/σ_b)
Load 1	B3S4	0.1	8250	150	1	200	338	0.60
	B3S5	0.1	8250	150	1	200	338	0.60
	B3S6	0.1	8250	150	1	200	338	0.60
Load 2	B2S2	0.1	6350	120	1	145	260	0.60
	B2S3	0.1	6350	120	1	145	260	0.60
	B3S11	0.1	6350	120	1	145	260	0.60
	B3S12	0.1	6350	120	1	145	260	0.60
	B3S13	0.1	6350	120	1	145	260	0.60
Load 3	B3S8	0.1	5420	100	1	133	222	0.60
	B3S9	0.1	5420	100	1	133	222	0.60
	B3S10	0.1	5420	100	1	133	222	0.60
Load 4	B2S8	0.1	11,000	0	1	0	451	0
	B2S9	0.1	11,000	0	1	0	451	0
	B2S10	0.1	11,000	0	1	0	451	0
Load 5	B3S1	0.1	0	120	1	145	0	∞
	B3S2	0.1	0	165	1	220	0	∞
	B3S3	0.1	0	200	1	266	0	∞

Table 2
Result of the tests conducted under various loading conditions.

Load case	Test ID	τ_{max} (MPa)	N_f (cycles)	L (mm)	L_{avg} (mm)	θ (°)	θ_{avg} (°)
Load 1	B3S4	388	30 195	2.1	2.4	49	48
	B3S5	388	26 233	2.65		48	
	B3S6	388	39 456	2.52		47	
Load 2	B2S2	305	82 584	4.56	4.2	46	45.8
	B2S3	305	84 159	4.92		47	
	B3S11	305	92 351	2.96		43	
	B3S12	305	55 586	4.18		47	
	B3S13	305	51 091	4.4		46	
Load 3	B3S8	257	301 869	6.35	5.8	43	42.3
	B3S9	257	296 964	6.51		42	
	B3S10	257	75 707	4.51		42	
Load 4	B2S8	251	54 476	–	–	–	–
	B2S9	251	393 132	–	–	–	–
	B2S10	251	76 135	–	–	–	–
Load 5	B3S1	145	$> 6.1 \times 10^5$	–	–	–	–
	B3S2	220	$> 4.1 \times 10^5$	–	–	–	–
	B3S3	266	$> 3.3 \times 10^5$	–	–	–	–

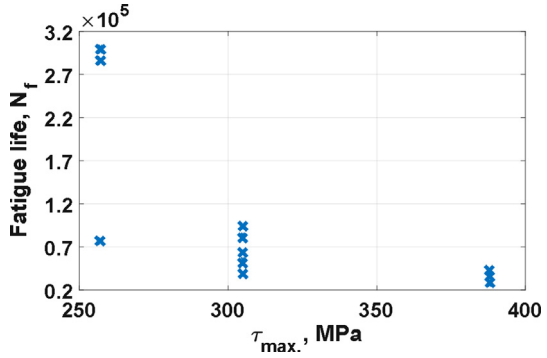

Fig. 4. Plot of total fatigue life against the maximum value of shear stress under in-phase bending-torsional loading.

3. Results and discussion

Initiation and propagation behavior of fatigue damage in Al 7075 were studied for pure bending, pure torsion, and in-phase multiaxial bending-torsion loadings. Initial tests were conducted with pure bending and pure torsional load conditions in order to gain better insight into the mechanisms governing the combined bending-torsional load and to segregate the effect of multiaxiality from uniaxial bending or torsional loading. Table 2 shows a summary of the experimental results for all the different load conditions. Load 4 and Load 5 correspond to the result of tests conducted under pure bending and pure torsion respectively; whereas, Load 1–Load 3 are the result of combined bending-torsion tests.

3.1. Fatigue life

In pure bending, multiple coupons were tested at a selected bending load (Load 4). The value of bending load was selected in order to conduct a low-cycle fatigue test ($N_f < \sim 10^5$ cycles) without getting a fatigue runout. For the pure bending tests conducted below the selected load (P_{max} = 8600 N), a fatigue runout was observed. Since, in all the cases, fatigue cracks nucleated on the plane of maximum shear stress range (explained in next section), fatigue life is discussed against the values of maximum shear stress obtained in each load condition, i.e. in pure bending, pure torsion, and combined bending-torsional loading. In case of combined bending-torsional loading (Load 1 - Load 3), the values of shear stress on a stress element at neutral axis was simply determined by adding the individual shear stress values calculated from the flexure formula and the torsion formula since both the loads were acting in-phase. As shown in Table 2, variability in fatigue life was observed for different specimens tested under the same loading condition in pure bending load (Load 4); whereas, specimens tested under pure torsional load exhibited fatigue runout and crack nucleation could not be observed, even though the maximum value of shear stress in pure torsion was higher than the shear stress in pure bending load.

For multiaxial in-phase bending - torsional loads, specimens were investigated at three different stress levels (Load 1–Load 3) as summarized in Table 2 and the variations in fatigue life are presented in Fig. 4. As shown in Fig. 4, higher fatigue life is obtained by reducing the value of maximum shear stress. An overall decrease of 34% in the shear stress value led to a six-fold increase in the average fatigue life. It is important to note that a high degree of scattering was observed in fatigue life at lower stress value, which was annihilated at a higher value of shear stress.

3.2. Crack nucleation

Since crack did not nucleate in the specimens tested under pure torsional load, the subsequent sections compare and contrast the results of the tests conducted under pure bending and combined bending-torsional loads. Fatigue crack developed under pure bending load is shown in Fig. 5. For all the tested coupons, a single crack nucleated on the surface of the specimen and was located on the plane of maximum shear stress (i.e. neutral axis), as shown in Fig. 5(b). For multiaxial in-phase bending-torsional load, fatigue cracks propagating under three different

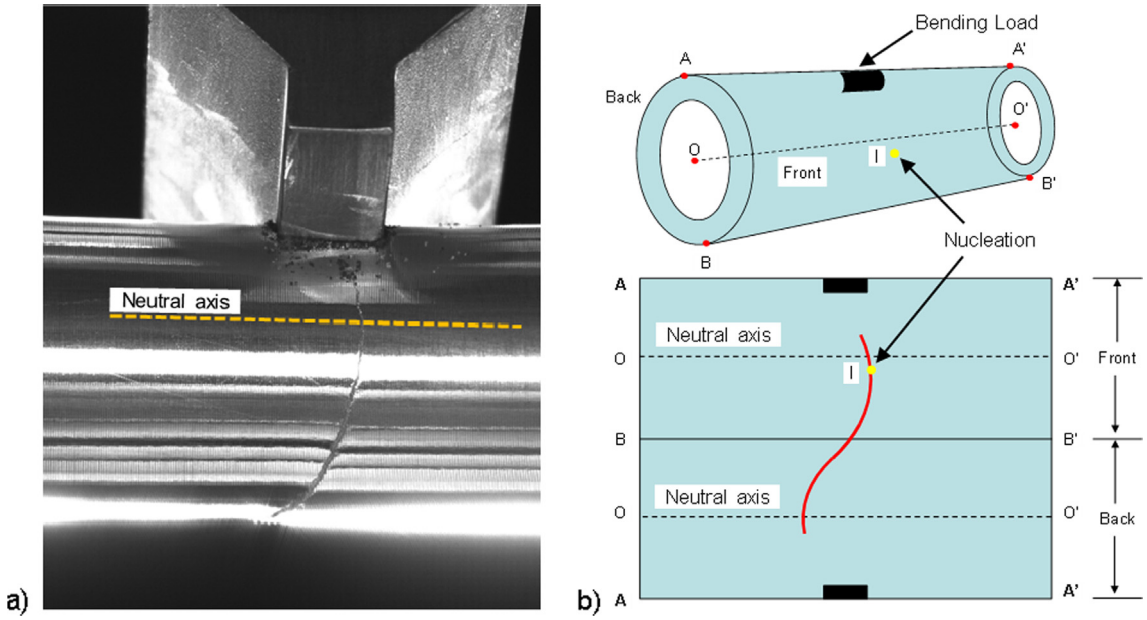

Fig. 5. (a) Actual crack trajectory, and (b) schematic of the crack trajectory for the failed coupons tested under pure bending load.

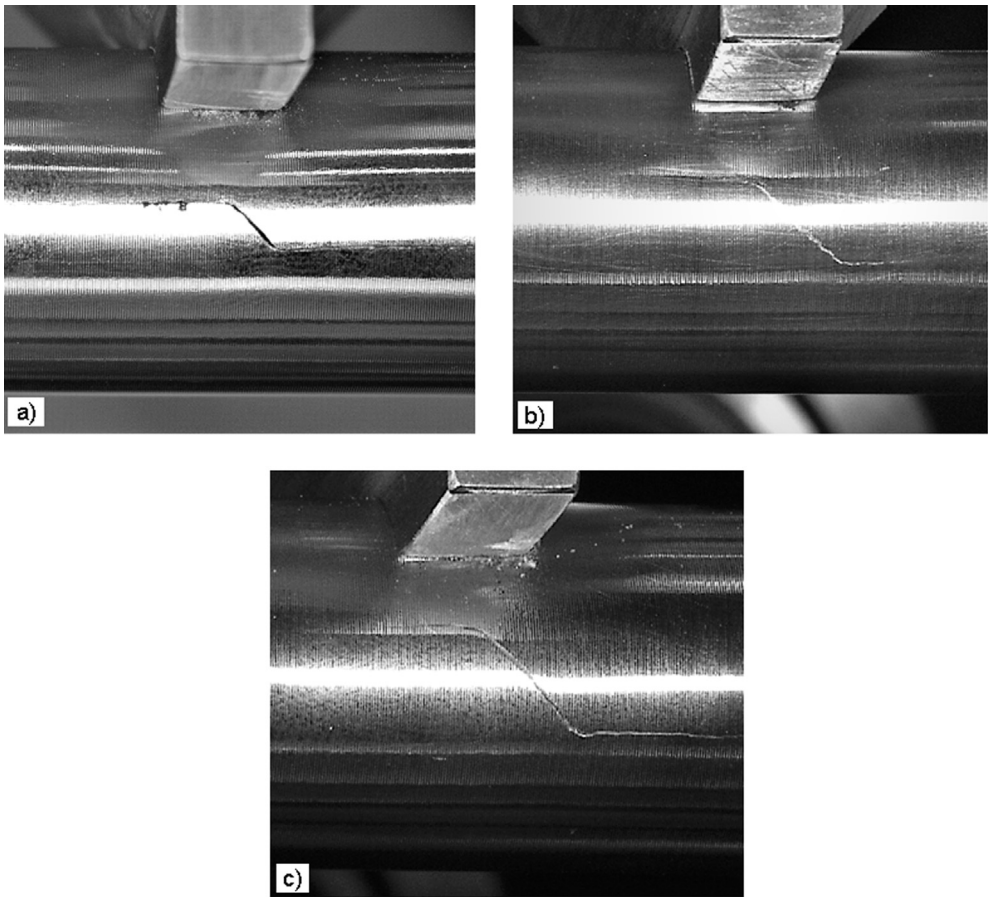

Fig. 6. Fatigue crack trajectory of the failed coupons tested under in-phase bending and torsional load for: (a) Load 1; (b) Load 2; and (c) Load 3.

stress levels are shown in Fig. 6. In all the tests, irrespective of the applied load magnitude, a single crack nucleated (at point I) on the surface of the specimen similar to the result of pure bending tests, as shown in Fig. 7(a). The crack nucleated at a point where the range of shear stress was maximum (i.e. plane of maximum shear stress). These observations along with the similarities in crack initiation showed by different types of loading emboldens the fact that the fatigue cracks in a pristine specimen tend to nucleate on the planes of maximum shear stress; and in a high strength material, such as Al 7075, fail by a single dominant microcrack. It is evident from the literature that smooth specimens of a ductile material can develop several microcracks leading to multiple nucleation sites; however, high strength materials and/or

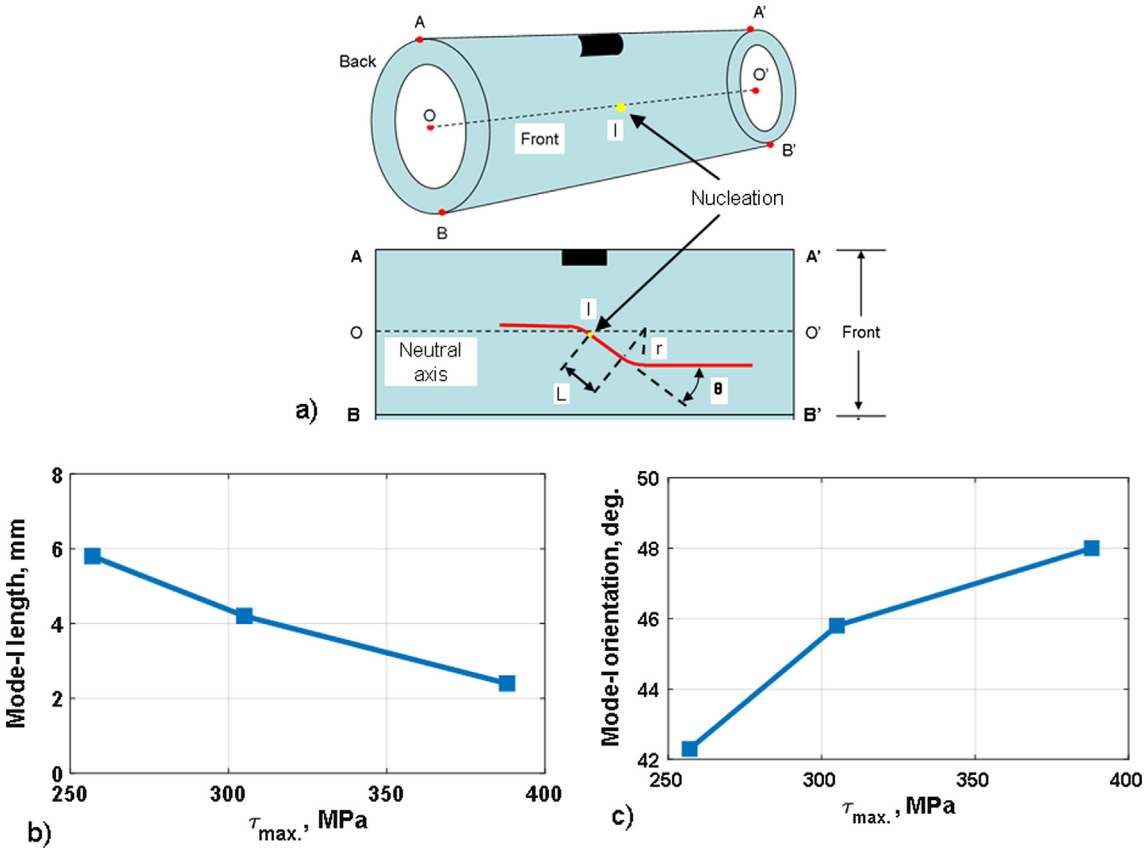

Fig. 7. (a) A schematic of the actual crack trajectory of the failed coupons tested under in-phase bending and torsional loading. (b) Average length of mode I dominant crack, and (c) Average orientation angle of crack is plotted against maximum value of shear stress in combined bending and torsional loading.

tubular specimens exhibit very low tendency to develop multiple crack initiation sites and thus fail by a single dominant crack [3,22]. Additionally, there is extensive experimental evidence [7,17,22,23] in literature supporting the hypothesis that naturally occurring fatigue cracks tend to initiate on planes of maximum shear stress.

3.3. Crack propagation

Crack propagation in fatigue fracture can be divided into three stages, i.e. stage I, stage II and stage III. Stage I corresponds to the immediate growth of crack following nucleation, which propagates on the plane of maximum shear stress for a very short distance (may or may not be visible on macroscopic scale), via mode II or/and mode III crack growth. In stage II, a stable crack growth is observed, which may propagate via mode I or mode II or mixed mode mechanism, depending on the applied stress-state. Stage III is the final stage in which unstable crack growth leads to fast fracture of the specimen.

Fig. 5 shows a fully developed crack trajectory of a representative specimen of the tests conducted under pure bending load. As shown in Fig. 5(b), crack traced the path to maximize mode II crack growth and predominantly grew on the planes of maximum shear stress in a continuously varying mixed mode condition. During the crack propagation, the value of ϕ_M changed from $\Pi/2$ (pure mode II) at the neutral axis to $\Pi/4$ at the specimen's bottom region. As shown in Fig. 5(b), an inverted S-shaped antisymmetric crack trajectory was obtained in which orientation of the crack with respect to longitudinal axis gradually deflected from approximately 90° at the neutral axis (front face) to approximately 45° at the bottom of the specimen (diametrically opposite to the applied bending load) and then again back to approximately 90° at neutral axis (back face). Since bending load introduces stress gradient (differently for shear stress and tensile stress) in the transverse direction, local value of λ and ϕ_M at crack tip continuously changed with crack propagation. As a result, continuous deflection of crack orientation was observed, leading to a curved trajectory.

Macroscopic fatigue cracks developed under combined bending-torsional load is shown in Fig. 7. As shown in Fig. 7(a), nucleation was immediately followed by a stable stage II crack propagation that defined crack trajectory and indicated different modes of crack growth (i.e. mode I, mode II or mixed mode). Clearly, the propagation behavior of the fatigue crack can be characterized by dividing the crack trajectory into three regions: mode I dominant mixed mode region, crack transition region, and pure mode II region. As shown in Fig. 7(a), orientation of the initial crack aligned closely with the maximum principal stress plane and thus showed mode I dominant growth. At the onset of stage II growth, initially, crack propagated on the plane of maximum principal stress, but because of the existing stress gradient (both for normal and shear stress) in the transverse direction, the magnitude and the direction of principal stress continuously changed at the crack-tip even though the crack propagated in its initially inclined direction. In other words, crack propagated in mode I dominant mixed-mode loading due to a monotonic increase in the local value of λ and ϕ_M at the crack tip. Once the crack reached a critical length, a gradual deflection in the crack tip was observed to maximize mode II crack growth, which turned the crack completely in the direction of the longitudinal axis. After deflection, the crack propagated in pure mode II through the entire length of the gauge region until specimen failure. Experimental evidences suggest that the mode of crack growth in a smooth specimen depends on multiple factors including material, load magnitude, stress amplitude ratio, initial crack tip condition, mean stress and anisotropy [5]. For a crack, growing in mixed mode load condition, it is difficult to predict the orientation of crack growth as the crack can continue to grow in mixed mode or can deflect either to shear

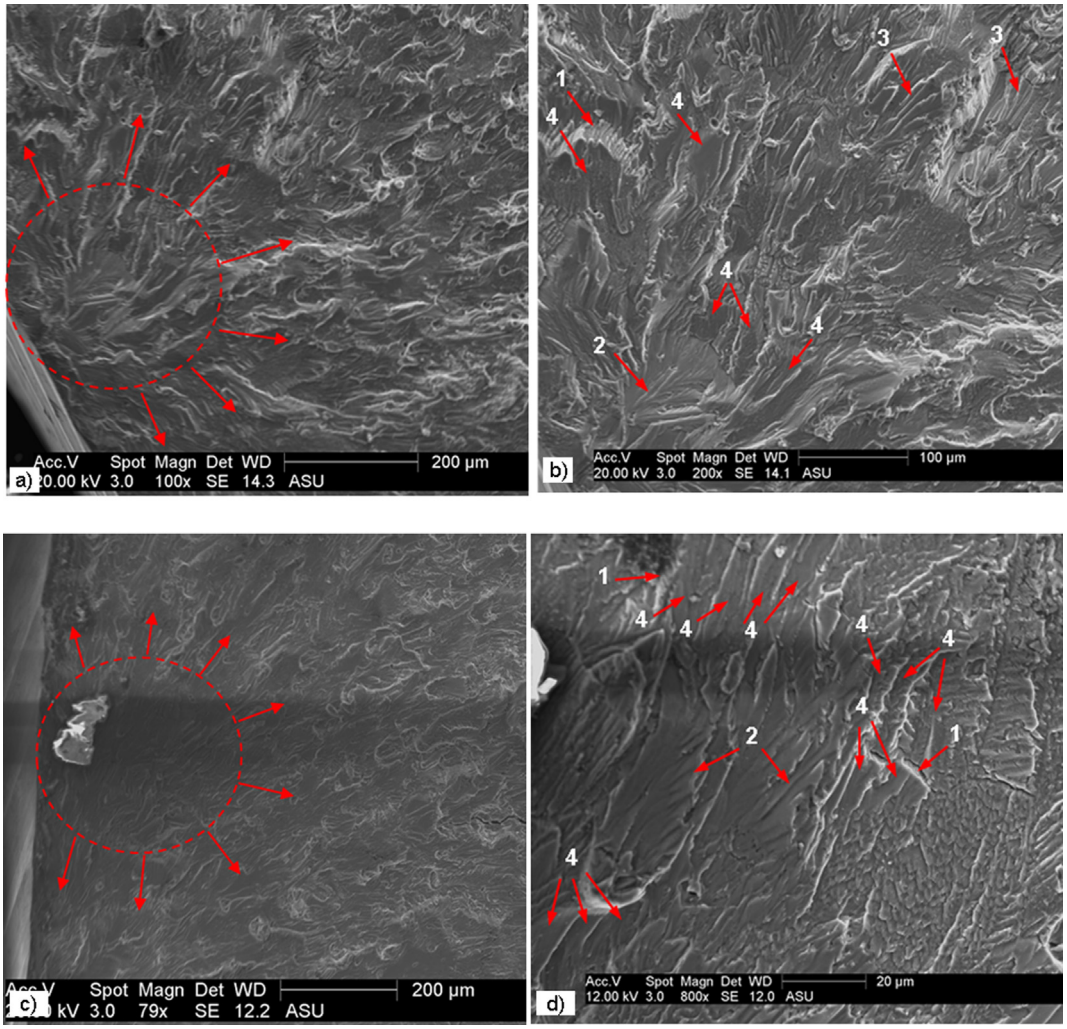

Fig. 8. Fracture surfaces of specimens showing nucleation and stage I growth during: (a) and (b) Load 1 condition; (c) and (d) Load 3 condition. Fracture features are marked: 1–flute, 2–feather marking, 3– serpentine glide, 4– cleavage steps.

mode or to tensile mode depending upon the stress state near the crack tip. Transition of crack to tensile mode (mode I) is shown in several fatigue studies in literature, while only a few studies have reported the transition of crack to shear mode [24]. It has been observed in the past that the crack preferably deflects to a shear mode growth only when two conditions are simultaneously satisfied at the crack tip: a) SIF in shear mode exceeded a critical value and; b) the value of λ or ϕ_M exceeded a critical value [5,17]. Since these critical values are sensitive to many parameters, such as material, microstructure, specimen geometry, crack-tip conditions, etc., quantitative information that could provide their accurate values has not been reported in literature.

3.4. Effect of magnitude

The effect of change in stress value was also investigated under multiaxial in-phase bending-torsional loading. A consistent behavior in fatigue crack initiation and crack trajectory was observed with various coupons tested under different sets of loading conditions mentioned in Table 1. It is important to note that despite having similarities in crack trajectories, magnitude of the applied load significantly affected the length of mode I dominant crack (L), orientation of mode I dominant crack (θ), and curvature of the crack deflection (Fig. 7). As shown in Fig. 7(b), the average length of mode I dominant crack increased with a decrease in the value of maximum shear stress. An overall decrease of 34% in shear stress led to an increase in average L by 1.4 times. On the other hand, the average value of crack orientation angle decreased with a decrease in maximum shear stress and is shown in Fig. 7(c). Here, a decrease in shear stress by 34% led to a decrease in the average value of θ by 12%. Moreover, deflection of the crack during crack transition became sharper as the testing load (maximum shear stress) was increased. These observations indicate that the mode mixity at the crack tip and the dominance of shear mode in the mixed mode crack growth increases with the increased value of applied load or maximum shear stress for the tests conducted at the constant value of λ.

3.5. Fractography

A scanning electron microscope (SEM) was used to analyze the fracture features of the failed specimens to correlate the fracture surface morphology with the initiation and propagation of the fatigue crack under various loading conditions (combined bending-torsional load). Several distinct features were observed on the fracture surface in the regions of crack nucleation, stage I propagation, and stage II propagation. A considerable variation in the fractographic features was also observed when the stress amplitude in the specimens was changed.

SEM images of a typical stage I fatigue fracture, including crack nucleation, at two different values of applied stresses (Load 1 and Load 3) are shown in Fig. 8. Irrespective of the applied stress level, stage I crack exhibited distinct features of cleavage fracture, such as river pattern, cleavage steps, facets, feather marking, flutes, and serpentine

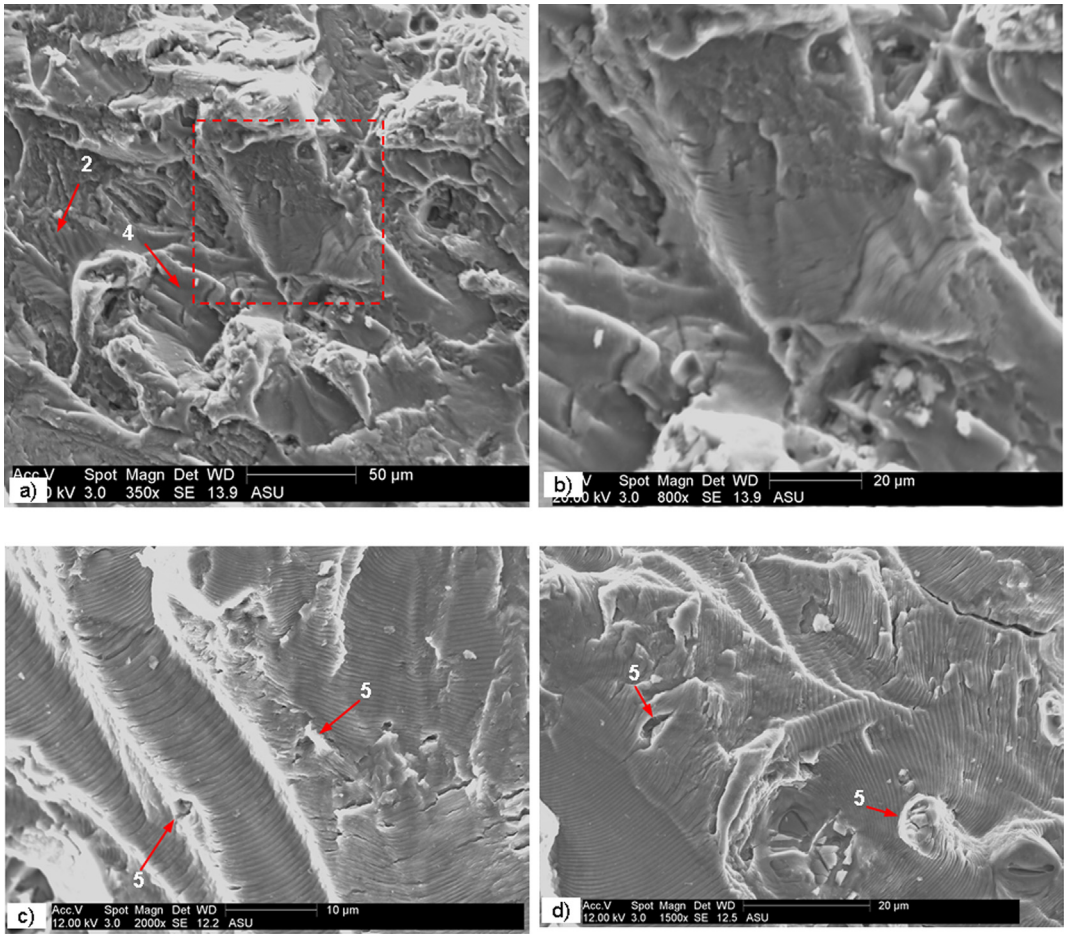

Fig. 9. Fracture surfaces of specimens showing stage II crack growth in segment-1 during: (a) and (b) Load 1 condition; (c) and (d) Load 3 condition. Fracture features are marked: 2–feather marking, 4–cleavage steps, 5–secondary crack.

glide, suggesting the brittle nature of fracture [25–27]. As shown in Fig. 8(a) and 8(c), cleavage fractures initiated on multiple parallel cleavage planes forming a river pattern and pointing back towards the origin of the fracture. Magnified pictures of the fracture surfaces reveal a highly tortuous path along with a higher degree of brittleness for the specimen tested under a higher stress value in comparison with that tested under lower stress value, as shown in Fig. 8(b) and 8(d). Among all the characteristic features, cleavage steps are most frequently observed and are spread across the entire region. Some of the large cleavage facets exhibited an array of very fine cleavage steps, also known as feather marking. Flutes, which are elongated grooves that connect widely spaced cleavage planes, are also observed on the fracture surfaces. Comparing the fracture surfaces under two different loadings, it was observed that these features tend to appear more frequently for higher values of applied stress.

Fracture surfaces during stage II crack growth were analyzed by dividing the crack region into two segments. Segment-1 represents the portion of stage II growth in which macroscopic crack propagated in mode I dominant mixed mode loading (between nucleation and start of crack turning), while segment-2 represent macroscopic crack propagation in mode II loading after crack turning (Ref. Fig. 7(a)). SEM images of segment-1 under two different stress levels, i.e. high stress (Load 1) and low stress (Load 3), are shown in Fig. 9. In Fig. 9(a) and 9(b), the characteristic features of the fracture surface at a higher stress value (Load 1) is illustrated, which clearly shows the presence of cleavage steps and feather marks, similar to that of stage I crack, in addition to the striation marks. It is important to note that the striations are partially developed and are present only in a few localized regions. A magnified SEM image, as shown in Fig. 9(b), clearly shows partial annihilation of these striations. Although the macroscopic crack appears to be mode I dominant, the SEM results of fractured surface indicate that the crack propagates in a mixed mode condition where the effect of mode II loading is significant. On the contrary, fracture surface at lower stress level (Load 3) exhibited well-developed, fully grown striations as shown in Fig. 9(c) and 9(d). Fig. 9(c) shows fatigue striations developed on different ridges, in which the walls of adjacent ridges are well connected with the continuously growing striations propagating in the same direction. However, variations in local stresses and microstructure can change the orientation of fracture plane and subsequently alter the direction of striation alignment, as shown in Fig. 9(d). Furthermore, secondary cracks were also observed at multiple locations, which were generated due to the interaction of inclusions / hard particles with the propagating striations. These observations agree with the result of macroscopic crack growth mode and support the fact that the crack growth is primarily dominated by mode I loading at a lower stress level.

Fig. 10 shows SEM images of segment-2 during high stress and low stress conditions. At higher stress, as shown in Fig. 10(a) and 10(b), fracture surface showed some interesting features. In addition to the cleavage steps, tongues were observed for the first time, which are formed when a cleavage fracture deviates from the cleavage plane and propagates a short distance along a twin orientation [25]. On magnification, distinct and periodic markings can be observed on the surface, which is also known as tire track and is shown in Fig. 10(b). These rows of parallel markings are the result of particles or protrusions on one surface being successively impressed into the surface of the mating half

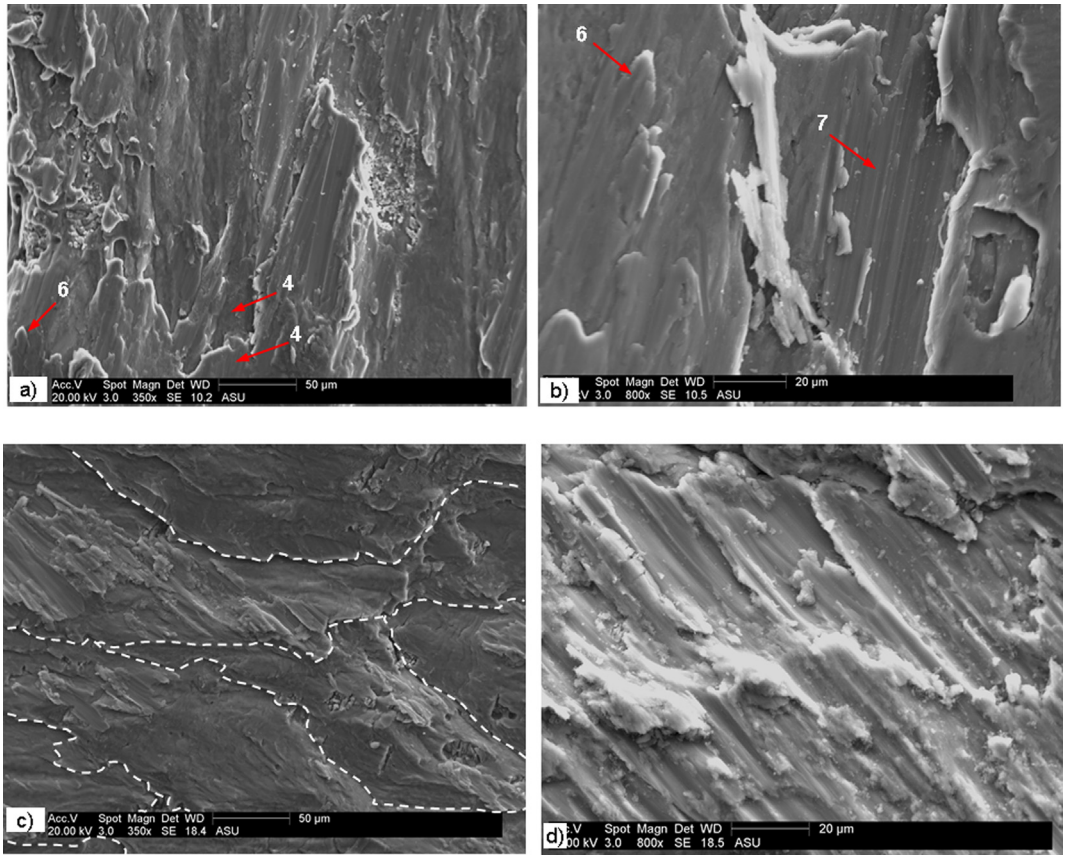

Fig. 10. Fracture surfaces of specimens showing stage II crack growth in segment-2 during: (a) and (b) Load 1 condition; (c) and (d) Load 3 condition. Fracture features are marked: 4–cleavage steps, 6–Tongue, 7–Tire track.

during the closing portion of the fatigue cycle in shear loading[25]. Unlike these observations, fracture surface at lower stress value predominantly showed an intergranular fracture, as shown in Fig. 10(c). Tire tracks were also observed at a higher magnification (Fig. 10(d)) but they were not continuously spread on the surface and were spotted only at very few locations.

4. Governing micromechanisms for fatigue-fracture behavior

Fatigue crack initiation in a smooth specimen is governed by several competing mechanisms that are dependent on various mechanical, microstructural and environmental factors. On the application of cyclic load, intrusions and extrusion emerge on the surface of the specimen forming persistent slip band (PSB). During the loading portion of the cycle, slip occurs on the crystallographically favored plane, i.e. plane having maximum value of critically resolved shear stress (τ_{CRSS}) or Schmidt factor (m); whereas, during unloading, reverse slip occurs on a parallel plane because the slip on the original plane is inhibited by the hardening or/and the oxidation of the newly formed free surface. These cyclic slips continuously form extrusions and intrusions, which in turn leads to PSBs. The interface between the PSB and the matrix is a plane of discontinuity across which there are abrupt gradients in the density and the distribution of dislocations. In that case, when the PSBs interact with the existing structural defects, such as second-phase particles/inclusions, grain boundaries, a highly stressed region is formed around the defects due to the accumulation of dislocations. Since the second-phase particles/inclusions are brittle and the matrix is ductile, crack is nucleated in a single shear when the critical elastic strain energy is reached inside the particle at the site of dislocation pile-up [6,28].

On the other hand, crack growth behavior can be influenced by distinct concurrent and mutually competitive mechanisms, which can act either ahead of the crack tip or in the wake region of the crack. These mechanisms may include: interlocking of fracture surface asperities, friction and roughness induced crack closure introduced by mode-mixity; crack tip blunting and strain hardening due to localized plastic deformation near the crack tip resulting in higher fracture toughness; crack closure caused by crack tip shielding due to compressive residual stresses ahead of the crack-tip; and plasticity induced crack closure caused by increased plasticity resulting from mode mixity at crack tip. With the growth of stage II crack, the component of mode II load, in mode I dominant mixed mode loading increased monotonically at the crack tip due to the presence of stress gradient along the transverse direction of the specimen. Since the size of the plastic zone in mode II is up to five times bigger than that in mode I for the same amplitude of far-field loading [6], an increase in mode II component of the load implied a larger plastic zone size at the crack tip as compared to the pure mode I load resulting in the attenuation of effective SIF, which is also the effective crack driving force. The larger size of the plastic zone was further manifested in the form of crack tip blunting, strain hardening, compressive residual stress and plastic wake, which in turn led to the enhancement of crack closure level and resulted in additional reduction in the effective SIF. When the crack reached to a certain critical length, where the value of ϕ_M was increased to a sufficiently higher value, the size of plastic zone became large enough to attenuate the effective SIF below the threshold SIF needed for the advancement of crack, which resulted in the crack arrest. After several fatigue cycles, the crack reinitiated on the crystallographically favored plane (maximum shear plane) deviating from its initial direction but grew only a small distance before being arrested again owing to the larger plastic zone resulting from the increased shear stress on new crack plane. This cycle of incremental deviation and growth followed by crack arrest and re-initiation was continued till the crack face

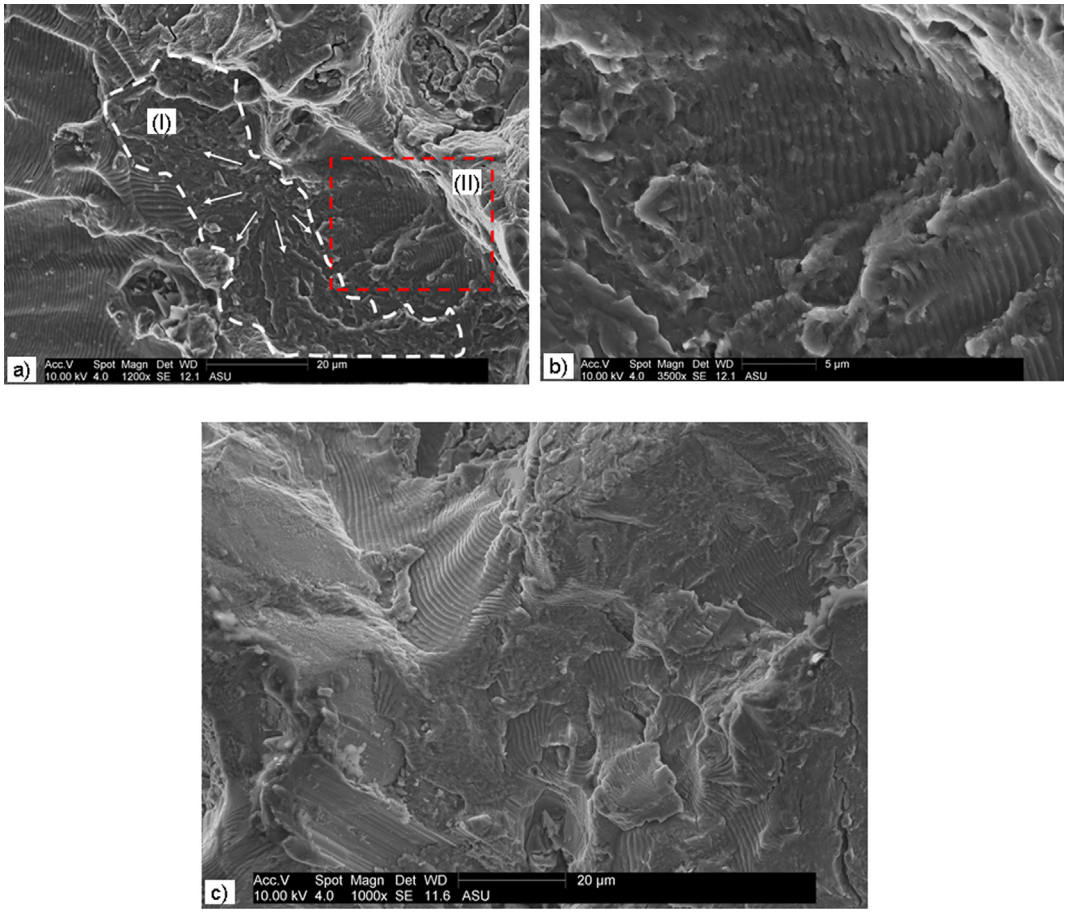

Fig. 11. Fracture surface topology in crack transition region of the specimen fatigued under Load 1 condition: (a) micrograph showing the regions of crack arrest and crack re-initiation; (b) Magnified image of region (II) showing stage II growth in re-initiated crack; (c) micrograph showing crack arrest and crack re-initiaion on the other mating half of the fracture surface.

became parallel to the longitudinal axis. With each incremental deflection, the local stress state at the crack tip changed due to the rotation of stress element resulting in higher value of shear stress or mode II component of loading. Once the crack became parallel to the longitudinal axis, the crack tip was exposed to pure mode II load having the maximum value of shear SIF that propagated the crack till failure. For the case when the applied external stress in the specimen was large, critical size of the plastic zone responsible for bringing the effective SIF below the threshold value was achieved at a smaller crack length, leading to the decrease in the length of mode I dominant crack as shown in Fig. 7(a). Because of the smaller crack length, a smaller value of crack tip opening displacement would occur resulting in an enhanced mode II induced crack closure. Furthermore, during the re-initiation phase of crack on the plane of maximum shear stress, the incrementally deflected crack experiences a higher increase in shear stress resulting in an increased plastic zone and more pronounced crack closure. Consequently, each time, crack re-initiation was followed by crack arrest after a relatively small growth, which led to a sharper deflection (smaller 'r') of mode I dominant mixed mode crack to pure mode II crack at higher stress levels as compared to the lower stress level, where a gradual transition (larger r) was observed.

The experimental evidence obtained from the investigation of fracture surfaces in crack transition region corroborates the proposed mechanism for crack turning from mode I dominant mixed mode growth to the pure mode II growth while capturing the effect of change in the magnitude of applied stress, as shown in Fig. 11. Fig. 11(a) depicts the entire phenomena involved in crack deflection process in a sequential manner (from left to right): crack arrest for mode I dominant crack propagation, crack re-initiation and stage I growth (region (I)), stage II crack propagation (region (II)). First, the crack propagated in mode I dominant load indicated by the well-developed and fully-grown striations traveling (left to right) on various planes, which suddenly stopped, implying crack arrest. Second, crack re-initiation occurred on an adjacent plane (region (I) in Fig. 11(a)) as indicated by the presence of river marking and small cleavage steps. Third, stage I propagation was immediately followed by stage II propagation (region (II) in Fig. 11(a)) as indicated by the formation of striations. An enlarged SEM image of stage II propagation is shown in Fig. 11(b), which shows a rapid increase in striation distance over a short distance. This sequence was repeatedly observed on the fracture surface supporting the proposed mechanism. Furthermore, investigations were also conducted on the other mating half of the fracture surface, as shown in Fig. 11(c), where the entire phenomena of crack deflection process were found to be repeated.

5. Conclusion and future work

Thin-walled tubular specimens of Al-7075 were investigated for fatigue crack initiation and propagation behavior under uniaxial loading (pure bending / pure torsion) as well as multiaxial in-phase bending-torsional load conditions. A single crack was nucleated on the plane of maximum shear stress for all the tests, except for pure torsion. The crack propagated in a continuously varying mixed mode load condition tracing an inverted S-shaped trajectory for pure bending load; whereas, the crack propagation in combined bending-torsional load was comprised of mode I dominant crack growth region followed by a crack

transition region, and pure mode II growth region. Furthermore, the micromechanisms governing crack initiation and propagation behavior under combined bending-torsional loading were identified and characterized. It was found that the nucleation is a shear-dominant brittle cleavage fracture, followed by a tortuous stage I growth. The degree of brittleness and the tortuous growth were further enhanced at the higher stress level. Stage II growth, before crack deflection, showed well-developed striations at lower stress level; and partially annihilated striations along with features of cleavage fracture at higher stress level. But the surface of the deflected crack showed features of intergranular fracture at lower stress level and transgranular fracture at higher stress level.

Further studies will be conducted to understand the effect of stress amplitude ratio and/or phase difference on the initiation and propagation behavior of fatigue crack. Another interesting aspect to explore would be the effect of load magnitude on the trajectory and orientation of crack under pure bending load.

Acknowledgements

The research is sponsored by the Army Research Laboratory through Cooperative Agreement W911NF-17-2-0207, Technical Program Manager Dr. Asha Hall

References

[1] Datta S, Chattopadhyay A, Iyyer N, Phan N. Fatigue crack propagation under biaxial fatigue loading with single overloads. Int J Fatigue 2018;109:103–13.
[2] Neerukatti RK, Datta S, Chattopadhyay A, Iyyer N, Phan N. Fatigue crack propagation under in-phase and out-of-phase biaxial loading. Fatigue Fract Eng Mater Struct 2018;41:387–99.
[3] Fatemi A, Gates N, Socie DF, Phan N. Fatigue crack growth behaviour of tubular aluminium specimens with a circular hole under axial and torsion loadings. Eng Fract Mech 2014;123:137–47.
[4] Tanaka K. Crack initiation and propagation in torsional fatigue of circumferentially notched steel bars. Int J Fatigue 2014;58:114–25.
[5] Qian J, Fatemi A. Mixed mode fatigue crack growth: a literature survey. Eng Fract Mech 1996;55:969–90.
[6] Suresh S. Fatigue of materials. (Cambridge University Press); 1998.
[7] Gates N, Fatemi A. Friction and roughness induced closure effects on shear-mode crack growth and branching mechanisms. Int J Fatigue 2016;92:442–58.
[8] May A, Taleb L, Belouchrani MAA. Analysis of the cyclic behavior and fatigue damage of extruded AA2017 aluminum alloy. Mater Sci Eng A 2013;571:123–36.
[9] Zhang J, Shi X, Bao R, Fei B. Tension–torsion high-cycle fatigue failure analysis of 2A12-T4 aluminum alloy with different stress ratios. IntJ Fatigue 2011;33:1066–74.
[10] Tanaka K, Matsuoka S, Kimura M. Fatigue strength of 7075–T6 aluminium alloy under combined axial loading and torsion. Fatigue Fract Eng Mater Struct 1984;7:195–211.
[11] Gough HJ, Pollard HV. The strength of metals under combined alternating stresses. Proc Inst Mech Eng 1935;131:3–103.
[12] Susmel L, Petrone N. Multiaxial fatigue life estimations for 6082-T6 cylindrical specimens under in-phase and out-of-phase biaxial loadings. European Structural Integrity Society, vol. 31. Elsevier; 2003. p. 83–104.
[13] Park J, Nelson D, Rostami A. Small crack growth in combined bending-torsion fatigue of A533B steel. Fatigue Fract Eng Mater Struct 2001;24:179–91.
[14] Park J, Nelson DV. In-phase and out-of-phase combined bending-torsion fatigue of a notched specimen. Multiaxial Fatigue Deform Test Predict ASTM Int 2000;1946:246–65.
[15] Branco R, Costa JD, Antunes FV. Fatigue behaviour and life prediction of lateral notched round bars under bending-torsion loading. Eng Fract Mech 2014;119:66–84.
[16] Nishihara T, Kawamoto M. The strength of metals under combined alternating bending and torsion with phase difference. Mem Coll Eng Kyoto Imp Univ 1945;11:85–112.
[17] Findley WN. Combined-stress fatigue strength of 76S-T61 aluminum alloy with superimposed mean stresses and corrections for yielding; 1953.
[18] Marciniak Z, Rozumek D, Macha E. Fatigue lives of 18G2A and 10HNAP steels under variable amplitude and random non-proportional bending with torsion loading. Int J Fatigue 2008;30:800–13.
[19] Niesłony A, Łagoda T, Walat K, Kurek M. Multiaxial fatigue behaviour of AA6068 and AA2017A aluminium alloys under in-phase bending with torsion loading condition. Materwiss Werksttech 2014;45:947–52.
[20] Davis JR. Aluminum and aluminum alloys. Light Met Alloy 2001;66.
[21] Richard HA. Specimens for Investigating Biaxial fracture and fatigue processes. Mechcanical Engineering Publications; 1989. p. 217–29.
[22] Shamsaei N, Fatemi A. Small fatigue crack growth under multiaxial stresses. Int J Fatigue 2014;58:126–35.
[23] Brown MW, Miller KJ. Initiation and growth of cracks in biaxial fatigue. Fatigue Fract Eng Mater Struct 1979;1:231–46.
[24] Yang Y, Vormwald M. Fatigue crack growth simulation under cyclic non-proportional mixed mode loading. Int J Fatigue 2017;102:37–47.
[25] Handbook ASM. Fractography, vol.12 (ASM international Materials); 1987.
[26] Kim WH, Laird C. Crack nucleation and stage I propagation in high strain fatigue—II. mechanism. Acta Metall 1978;26:789–99.
[27] Cina B, Kaatz T. A systematic study of the fractography of fatigue in high strength aluminium alloys. Fatigue Eng Mater Struct 1979;2:85–95.
[28] Meyers MA, Chawla KK. Mechanical behavior of materials; 1999.